Mapping visual spatial prototypes: Multiple reference frames shape visual memory

Elena Azañón[a,b,c,d,*,1], Raffaele Tucciarelli[a,1], Metodi Siromahov[a,e], Elena Amoruso[a], Matthew R. Longo[a]

[a] Department of Psychological Sciences, Birkbeck, University of London, WC1E 7HX London, United Kingdom
[b] Institute of Psychology, Otto von Guericke University Magdeburg, 39106 Magdeburg, Germany
[c] Center for Behavioral Brain Sciences, 39106 Magdeburg, Germany
[d] Department of Behavioral Neurology, Leibniz Institute for Neurobiology, 39118 Magdeburg, Germany
[e] Department of Psychology, Royal Holloway, University of London, TW20 Egham, United Kingdom

A B S T R A C T

Categories provide a fundamental source of information used to structure our perception of the world. For example, when people reproduce the remembered location of a dot in a circle, they implicitly impose vertical and horizontal axes onto the circle, and responses are biased towards the center of each of the resulting quadrants. Such results reveal the existence of *spatial prototypes*, which function as Bayesian priors and which are integrated with actual memory traces. Spatial prototypes have been extensively investigated and described in previous studies, but it remains unclear what type of information is used to create spatial categories. We developed a new approach that allowed to 'image' patterns of spatial bias in detail, and map the internal representational structure of objects and space. Previous studies, using circular shapes suggested that boundaries are established based on a viewer-based frame of reference, therefore using cues extrinsic to the object. Given that a circle has radial symmetry, the axes imposed cannot come from the shape itself. Here we investigated if the same applies for shapes with clearly-defined symmetry axes and thus intrinsic frames of reference. Using rotated shapes (squares and rectangles), where extrinsic and intrinsic cues are dissociated, we observed flexible usage of multiple reference frames. Furthermore, in certain contexts, participants relied mostly on cues intrinsic to the shape itself. These results show that humans divide visual space as a function of multiple reference frames, in a flexible, and context dependent manner.

1. Introduction

Categories provide fundamental information to structure our perception of the world (Harnad, 1987). In the case of space, research has demonstrated systematic biases in the reproduction of remembered spatial locations, suggesting that memory for actual stimuli is integrated with central categorical information about where stimuli are expected to be (i.e., spatial prototypes; Cheng, Shettleworth, Huttenlocher, & Rieser, 2007; Huttenlocher, Hedges, & Duncan, 1991; Newcombe & Huttenlocher, 2000). In this way, categories function as "perceptual magnets", pulling in nearby stimuli (Kuhl, 1991). For example, when reproducing the remembered location of a dot in a circle, observers' responses are biased towards the centroids of four imaginary quadrants (Huttenlocher, Hedges, Corrigan, & Crawford, 2004;

Huttenlocher *et al.,* 1991; see also Taylor, 1961). Though the use of spatial prototypes introduces bias towards the mean value, or prototype, of the category, it can nevertheless reduce overall error when memory is imprecise (e.g., "the dot was in the top left quadrant"; Duffy, Huttenlocher, & Elizabeth Crawford, 2006; Huttenlocher *et al.,* 2004). Studying the pattern of bias for stimuli at varying locations across a shape is a potentially powerful tool to map the internal structure underlying spatial representation of objects, i.e., how spaces are broken up into categories, or organized in memory. To achieve a more detailed description of this structure than provided by previous work, we developed a novel method of 'imaging' this representation.

In the example of the circle above, there is no reason to think that stimuli are actually more likely to appear in the center of each quadrant, yet responses are nonetheless biased towards those locations. This

---

* Corresponding author at: Institute of Psychology, Otto von Guericke University Magdeburg, Universitätsplatz 2, 39106 Magdeburg, Germany.
  E-mail addresses: eazanyon@gmail.com, elena.azanon@ovgu.de (E. Azañón).
  [1] Both authors contributed equally.

suggests that circles are spontaneously organized into quadrants, by imposing vertical and horizontal axes. Attraction towards categorical prototypes has been shown for a variety of tasks and stimuli, such as urban landmarks (Sampaio & Cardwell, 2012), object location within a room (Sargent, Dopkins, & Philbeck, 2011), or toys hidden in sandboxes (Huttenlocher, Newcombe, & Sandberg, 1994; Newcombe, Huttenlocher, & Learmonth, 1999). However, the actual distribution of prototypes for a given object, as well as its categorical structure, has been often overlooked, for instance by assuming a particular number of fixed prototypes (e.g., Wedell, Fitting, & Allen, 2007) or considering only one type of response bias (e.g., Huttenlocher et al., 1994). This is the case for instance of studies where participants are asked to retrieve from memory the location of a dot or an object within a rectangle, but only bias in the right-left direction is modelled (Huttenlocher et al., 1994; Spencer, Simmering, & Schutte, 2006), which may underestimate the number of prototypes involved.

In the present study, we developed a new method of characterizing the pattern of spatial prototypes in a data-driven way, by assessing the pattern of directional biases across an entire shape. Specifically, our method quantifies the extent to which each location in a given shape attracts or repels location memory, without making a priori assumptions regarding the categorization of space or number of prototypes. This method allows to image the internal representational structure of objects with a level of detail never previously reported, including the imposition of partition axes (e.g., the vertical and horizonal axes in the circle).

The way shapes are divided and hence categorized will vary depending on the frame of reference used by the observer. Egocentric reference systems, for instance, are those in which locations are specified with respect to the observer, such as the retina, the head, or the body, whereas allocentric (or environmental) ones are independent from the observer, such as gravity or landmarks within a room (Fitting, Wedell, & Allen, 2005). Intrinsic reference frames, on the other hand, are object-based, and defined through the object's intrinsic axes and boundaries (McNamara, 2003; Mou, Fan, McNamara, & Owen, 2008; Mou, Xiao, & McNamara, 2008; Wang, Sun, Johnson, & Yuan, 2005). Given that the vertical and horizontal axes in our experiments can be defined with regard to both egocentric and allocentric systems, we have opted to define these axes as *extrinsic* vertical and horizontal when they are aligned or perpendicular to gravity, respectively, in direct opposition to the object *intrinsic* axes (which might or might not be aligned with the extrinsic ones).

The widespread use by participants of the extrinsic vertical when segmenting shapes into categories has led several authors to argue that a universal division of space, imposing vertical (and often horizontal) boundaries, forms the basis for spatial categorization (Engebretson & Huttenlocher, 1996; Huttenlocher et al., 2004; Wedell et al., 2007). The underlying idea is that vertical and horizontal orientations are most exactly represented by the visual system (Huttenlocher et al., 2004) as stimuli aligned with the vertical and horizontal axes are perceived more accurately (Appelle, 1972) and faster (Palmer & Hemenway, 1978) than intermediate orientations, a phenomenon known as *oblique effect*. Hence, categorization under cardinal axes, i.e., the segregation of locations pertaining to one or another category, should be more precise (Engebretson & Huttenlocher, 1996; Huttenlocher et al., 2004). However, this might be particularly the case for structures like the circle, where the axes imposed can only come from ego- or allocentric reference frames, given the circle's radial symmetry. It is nonetheless possible, that for shapes with clearly-defined symmetry axes, intrinsic reference frames might play a bigger role than previously thought. Indeed, a large body of evidence from complementary areas of research in spatial cognition suggests that people organize spatial relationships, e.g., between several items in a frame, based on a flexible combination of allocentric, egocentric, and intrinsic reference frames (Tamborello, Sun, & Wang, 2012). Indeed, there is a long-standing literature in object recognition, building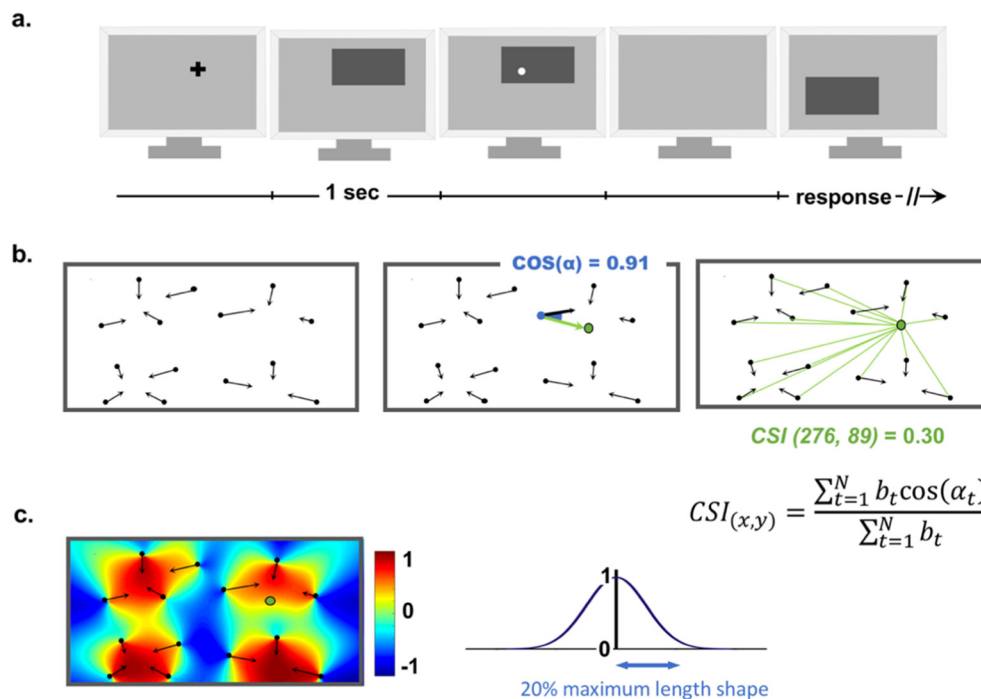 on Marr's initial ideas, which have shown that objects are represented in memory in an intrinsic (object-based) reference system, in which object parts and features within objects are specified relative to the intrinsic axes of the object (Marr, 1982; Marr & Nishihara, 1978) or other object parts (Lowe, 1987). Moreover, while it has been shown that the addition of allocentric reference cues at the boundary of a circle (e.g., marks added on the perimeter of a circle) does not change the typical way extrinsic vertical and horizontal axes are imposed, it does so, when the cues are considered to be intrinsic to the shape, e.g., when cues and circle rotate together on a trial basis (Fitting, Wedell, & Allen, 2007).

The role that intrinsic reference frames plays in the categorization of shapes for memory of spatial location is unknown. Indeed, only a few studies have considered the category structure of shapes other than circles (e.g., Langlois, Suchow, & Griffiths, 2017; Schmidt, 2004; Wedell et al., 2007), with inconclusive results about the weight given to each frame of reference. Wedell et al. (2007), for instance, tested several shapes, finding a pattern of biases consistent with the use of an extrinsic frame of reference, with four prototypes reflecting, as in the circle, four spatial quadrants generated by imposing vertical and horizontal boundaries. However, as none of the figures were rotated, the results are also consistent with an intrinsic reference system (i.e., based on axes of symmetry). Indeed, using the same shapes, but with a different approach (i.e., through serial reproduction, where localization errors are transmitted from person to person) and with substantially better resolution, Langlois et al. (2017) found that the pattern of biases varied depending on the number of corners of each shape, consistent with the use of an intrinsic reference system. Nonetheless, the actual role of the extrinsic reference frame was not tested. Indeed, both intrinsic and extrinsic reference frames might play a role in the pattern of error localization from memory. In this regard, Schmidt (2004) tested configurations of three dots (forming invisible triangles) and calculated the degree of symmetry in the pattern of error localization across two halves of the triangle for each of the different symmetry axes. He found that the degree of symmetry was determined by the intrinsic reference system of the landmark configuration as well as by the extrinsic vertical axis. Thus, while symmetry was best near the cardinal axes of the landmark system irrespective of their orientation (denoting the use of an intrinsic reference frame), symmetry of non-cardinal axes was enhanced when aligned with the extrinsic vertical. While this study reveals the common use of several reference frames, it does not provide insight into the actual categorical structure of memory biases.

In this paper, we had two main aims. First, we aimed to develop a method for 'imaging' the detailed internal structure underlying spatial representation of objects, by mapping the pattern of mislocalisations across the shape. The proposed method is able to quantitatively index a location or a region's salience (attracting or repelling) in a person's overall spatial representation of an object, and test their reliability statistically across subjects, and against a null hypothesis. Moreover, contrary to previous methods, it allows imaging of categorical boundaries, which can help disambiguate the contribution of extrinsic and intrinsic reference frames. Second, we aimed to determine the reference frames in which spatial categories operate, and in particular to assess the general view that space is mostly divided by imposing vertical and horizontal boundaries (e.g., Engebretson & Huttenlocher, 1996). To dissociate the influence exerted by each reference system, we mapped the internal representational structure of a shape in two orientations, i.e., a non-rotated square and a square rotated 45°. This allowed the shapes to maintain the same intrinsic axes of symmetry, while varying the alignment with the extrinsic vertical and horizontal.

2. Experiment 1: imaging spatial categories, a new approach

We developed a novel way to characterize the pattern of spatial prototypes used to reproduce from memory the location of dots within a shape. In Experiment 1 we validated the method by testing localization biases from memory of dots inside a rectangular shape. By assessing the

a.

b.

c.

$$CSI_{(x,y)} = \frac{\sum_{t=1}^{N} b_t \cos(\alpha_t)}{\sum_{t=1}^{N} b_t}$$

Fig. 1. Experimental logic to image the categorical structure of a shape. (a) Procedure. Participants saw a grey shape (here, a rectangle) for 1 s in which a white dot appeared for another second. The shape disappeared and after a delay of 1 s, it re-appeared at a different location. Participants used the mouse cursor to indicate the location within the shape where the dot had appeared. In Experiments 2 and 5, the first panel of 1a was blank. The distribution of dot locations was selected once pseudo-randomly with no overlap across the dots, and presented to each participant in random order. The shape of the figure, size and number of trials changed across experiments. All dots in the figure are magnified for illustrative purposes. (b) Mean cosine similarity index (CSI). Left panel. Error vectors of one hypothetical participant (note that in reality there were 395 dot locations in Experiment 1, rather than 14 as in the example). The black dots correspond to the target dot locations, and the tip of the arrows to the location reproduced from memory by the participant. Middle panel. Predicted error vector (in green) for one target location (blue dot) if the location depicted by the green dot (randomly selected) was influencing entirely the location from memory of that particular target location. To quantitatively index this influence, we calculate the cosine of the angle formed between the predicted and error vector, as a measure of directional similarity. If both errors follow the same direction, the cosine of the angle will be 1, 0 if they are orthogonal and −1 if they follow opposite directions. Right panel. Given that we had 395 target locations (14 in this example), we can calculate the extent of attraction of that location (green dot) across the neighbouring target dots (hereafter, cosine similarity index, CSI). To do so, we calculated all the cosines of the angles formed between predicted and observed error vectors and then weighted each cosine (14 in the example) using a Gaussian window. This procedure gives more weight to those target dots that are closer to the predicted location (green dot). (c) Similarity map. To create the similarity map, we repeated the procedure explained in the right panel of Fig. 2b, iteratively for each pixel inside the shape. We then plotted each similarity index obtained for each pixel in the rectangle. Thus, each CSI (ranging from −1 to 1) indicates the amount of attraction (indices > 0) or repulsion (indices < 0) at each location. On the right side it is depicted schematically, the Gaussian window used to weight each cosine value. In the formula, x and y denotes pixel cartesian coordinates and b_t the weight given to each cosine with angle α_t. (For interpretation of the references to colour in this figure legend, the reader is referred to the web version of this article.)

pattern of directional biases across the entire shape, we aimed to assess, in a data-driven way, which regions tend to attract remembered location (i.e., spatial prototypes), and which tend to repel memory (i.e., spatial *anti-prototypes*). In particular, we developed a statistical method that produces for each given location within a shape a cosine similarity index (CSI) that quantifies the extent to which that location either attracts or repels location memory, and allow to evaluate statistically these biases. Thus, by colour-plotting CSI values across locations, we can image the internal category structure of a shape. The calculation of the CSI is depicted in Fig. 1b.

2.1. Methods

2.1.1. Participants

Twenty volunteers participated in Experiment 1 (M = 29.60 years old, SD = 6.30, 11 females). Participants were naïve as to the purpose of the experiment and received monetary compensation or course credit. Participants provided informed consent, and the procedures were approved by the local committee and were in line with the principles of the Declaration of Helsinki.

2.1.2. Materials and procedure

Stimuli were presented on a 24-inch computer screen with a light grey background (1920 × 1200 pixels resolution, 60 GHz refresh rate), placed about 60 cm in front of the participant. The stimuli consisted of white dots (0.26° degrees of visual angle [°] in diameter, 10 pixels) presented inside a dark grey rectangle (24.5° × 12.4°, 960 × 480 pixels). The location of the rectangle varied randomly across the computer screen, and the dot could appear in one of 395 different locations

inside the rectangle. The distribution of dot locations inside the rectangle was identical across participants and the 395 dots were presented one by one in random order. Five extra dots were presented at the beginning of the experiment as practice trials and were not analysed. The distribution of dot locations was selected pseudo-randomly, at the beginning of the experiment, aiming at creating a visually uniform distribution of locations with no overlap across the dots. The minimum distance across dots was set to 15 pixels (from their centres), and no dot could appear within 8 pixels from the edges. We presented the task in Matlab running in full screen using Psychtoolbox (Kleiner, Brainard, & Pelli, 2007).

On each trial, a black fixation cross appeared at a random location of the screen, and was replaced after a second by a rectangular shape (see Fig. 1a). After a delay of 1 s, a white little dot appeared within the shape for 1 s (i.e., encoding interval). Then, the shape and the dot disappeared for 1 s (i.e., retention interval) and an identical shape re-appeared without the dot in a new random location on the screen (retrieval period). At this point, participants were requested to localize, without time restriction, the relative position of the white dot on the new rectangle, using the mouse cursor (crossed-shaped). The mouse cursor appeared together with the last shape in a random location within the screen. The Experiment lasted about 1 h, and participants rested every 50 trials.

2.1.3. Analyses

Error vectors and Predicted vectors. We developed a statistical method that produces for each given location within a shape a CSI (cosine similarity index) which quantifies the extent to which that location either attracts or repels location memory. CSIs rely on the

similarity between the direction of two types of error vectors: error and predicted error vectors. Error vectors (black lines in Fig. 1b) are computed as the difference in pixels between the central location of the target dots (black dots in Fig. 1b, n = 395) and the dot locations reported from memory by the subject (arrow tips in Fig. 1b). Note that for each participant we have at most 395 error vectors. This is formally described by the following formula:

$$Error\ Vector_{xy} = Response_{xy} - Target_{xy} \qquad (1)$$

An error vector with a length equal to zero indicates that the participant correctly reported the position of the dot. An error vector with a length greater than zero indicates that the dot was mislocalized and the greater the length, the greater the error. Importantly, the arrow also provided the direction of the error. Predicted error vectors (green lines in Fig. 1b), on the other hand, are computed as the difference between the location of a given pixel (green dot in Fig. 1b) and the location of each target dot. Thus, each pixel in the rectangle (960 × 480) is once treated as a predicted attractor or prototype. The predicted error vector corresponds to the predicted direction of the error vector if the bias was directly towards that particular pixel. Note that for each given pixel and participant, we can calculate 395 predicted vectors. This is formally described by the following formula:

$$Predicted\ Vector_{xy} = Pixel_{xy} - Target_{xy} \qquad (2)$$

Cosine similarity index calculation and depiction of similarity maps. For each participant, we calculated iteratively one CSI value for each pixel in the rectangle (for a total of 960 × 480 pixels). However, the method could be applied with either a lower or a higher spatial resolution (i.e., using more or fewer pixels; see Fig. 1 for a description of the procedure). We used all participant's 395 responses, regardless of the magnitude of the error, excluding only those responses that were made outside the shape (0.25%). On each iteration (from tested pixel xy = [1,1] to xy = [960, 480]), we first computed the direction of the predicted vectors from the 395 target dots to the tested pixel (Eq. 2). Second, for each target dot we calculated the cosines of the angles formed between the observed and predicted error vectors. A cosine of 1 indicates that the direction of the error vector was that of the predicted vector and −1 indicates the opposite direction. Third, we weighted each cosine using a Gaussian window, giving more weight to target dots closer to the given pixel (see below for further details). Fourth, we obtained a CSI for the tested pixel by computing the weighted mean across the ~395 cosine values. Formally, we used the following formula to compute the CSI at each pixel:

$$CSI_{xy} = \frac{\sum_{t=1}^{N} b_t \cos(\alpha_t)}{\sum_{t=1}^{N} b_t} \qquad (3)$$

CSI_p indicates the CSI at the tested pixel defined by *xy* coordinates. The sum considers the contribution of all N targets. b_t indicates the weight given to the cosine with angle α_t, which is the angle between the observed error response and the vector that links the target to the pixel *p*.

We repeated the above steps for each pixel in the figure and depicted each CSI on a colour map (i.e., similarity maps). Each CSI (ranging from −1 to 1) quantifies the amount of attraction or repulsion exerted by the location of that pixel on nearby responses. If neighbouring pixels of certain locations show higher (or lower) cosine values than other locations, then those regions have a special status as they would "attract" (or "repeal") the responses more than other locations, and they can be considered as prototypes (or anti-prototypes); alternatively, if there are no locations showing cosine values in a systematic way, this would be an indication that there are no prototypes in the figure.
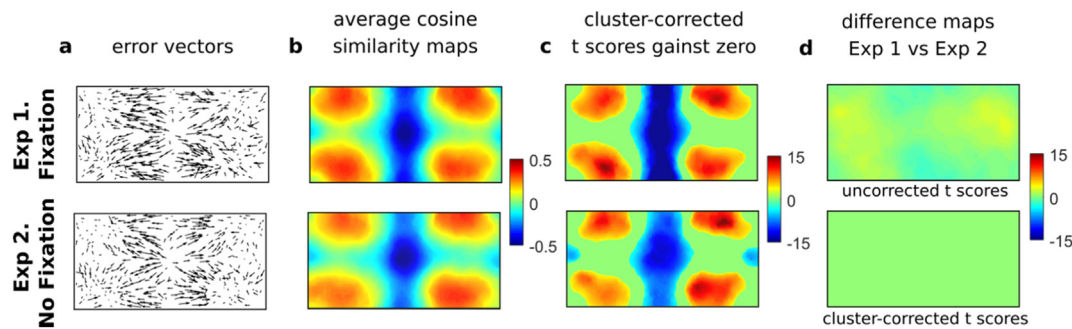
Gaussian Window. As noted above, we introduced a weighting based on the vicinity of the current pixel, assuming that neighbouring targets are more attracted than targets farther away from the current

pixel. If more than one prototype exists in a given shape, this procedure facilitates their visualization. Indeed, by applying the same weight to all targets one might risk cancelling out the emergence of different prototypes. The Gaussian window (w) was defined as $w(n) = e^{-n^2/2\sigma^2}$, where the standard deviation corresponds to σ = (L − 1)/(2α). L, as the window length, was set to the maximum length of the shape (here, the diagonal of the rectangle). α was set to 10.78 pixels and kept constant across experiments. Note that and α of 10.78 pixels produces a Gaussian window where the most informative range of weights (ranging from 1 to 0.1) are given to distances that are shorter than 20% of the maximum shape length (i.e., L).

Testing the reliability of similarity maps across participants. In order to evaluate whether the mean similarity map showed CSIs that were significantly different from zero, we ran a one-sample *t*-test for each CSI across participants. Note that we had to run a large number of statistical tests which increased the false alarm rate. To control for this issue, we adopted a cluster-based permutation analysis with Monte Carlo, which is a popular method to control for Type I error in the neuroimaging community and it is used both in functional magnetic imaging and magneto- (or electro-) encephalography studies (Maris & Oostenveld, 2007; Nichols & Holmes, 2002). The maps that we obtained from the cosine similarity analysis were comparable to the brain functional images with the difference that our fundamental unit was a two- rather than a three-dimensional pixel. The algorithm searched for clusters of pixels (i.e., neighbouring pixels that show similar results) and then evaluated if the observed clusters were significantly different from zero. Specifically, neighbouring pixels were considered as a cluster if their individual *t* values were higher than the critical value ($p < 0.001$; $T_{crit}(19) = 3.58$) and they shared at least one vertex. Then, we computed the cluster statistic which was the sum of the individual values of the pixels that were part of that cluster. To ensure that the observed cluster values were not due to chance, we repeated the procedure 5000 times but flipping, at each iteration, the signs of the CSIs of randomly selected subjects before computing the statistics for each pixel. In this way, we built a null distribution that served as a criterion to select significant clusters. Specifically, we counted the number of times a permuted cluster statistic exceeded the observed cluster value. We thus obtained the probability (*p* value) associated with the observed clusters by dividing the number of times a permuted value was greater than the observed value for the number of iterations. Only those observed clusters which were exceeded by the permuted values < 5% of the times ($p < 0.05$) were considered significant.

Model-based analyses to test the rectangle skeleton. Finally, as it has been previously proposed that people might spontaneously divide a rectangular shape using two inward triangles at the sides of the figure and a horizontal line in the middle connecting the two vertices, i.e., the so-called rectangle skeleton (Fig. 3b, first graph bar, Firestone & Scholl, 2014) we also conducted a model-based analysis on the data. We use the term model-based analyses in contraposition to the term data-driven analyses used for our main analyses. We evaluated specifically a predicted model of shape structure, in particular the shape skeleton. Thus, we assumed the existence of 4 fixed prototypes in the centroids of the four presumed categories emerging when using the rectangle skeleton. In order to do so, we selected for each of the four presumed prototypes the target dots whose distance to each prototype was smallest. We used these dots and their error vectors to calculate the averaged cosine similarity for each prototype. We used an identical procedure as in the main analyses, but this time without weighting by the distance of the target location to the prototype. This is because just one to four prototypes (depending of the model) are tested rather than over 400,000 (960 × 480) as in the main analyses. Therefore with a wighting procedure based on target distance to prototype, only the closest targets would have been taken into account. Here, instead, we weighted each cosine by the length of its error vector (giving more weight to those errors that were larger). The same procedure without any weighting procedure produced a very similar patern of results. The

Fig. 2. Results of Experiments 1 (top row) and 2 (bottom row). (a) Mean actual error vectors across participants obtained for each response. Each vector is calculated as the difference between the target dot location, represented by the origin of the arrow, and the participant's response, represented by the tip of the arrow. (b) Cosine similarity indexes (CSIs) averaged across participants. Positive values indicate systematic response biases towards these locations. Negative values indicate systematic biases away from these locations. (c) One-sample t-statistics against zero for each location across participants with cluster correction for multiple comparisons. (d) Two-sample t-statistics between Experiments 1 and 2, depicting uncorrected (top panel) and cluster corrected t scores for multiple comparisons (bottom panel).

four CSI were then averaged to obtain a single CSI per participant. The averaged CSI across participants were then submitted to a one-sample *t*-test against zero. For completeness, we repeated these analyses using as prototypes the center of mass of each quadrant (imposing vertical and horizontal boundaries, i.e., the centroids), the geometrical center of the rectangle, and the center of each halve as if the rectangle would have been divided into two by a vertical line through the middle. For these analyses, we excluded from the analyses participants' responses that were made outside the shape (0.25%) or were 3 SD above each participants' response mean (1.48%).
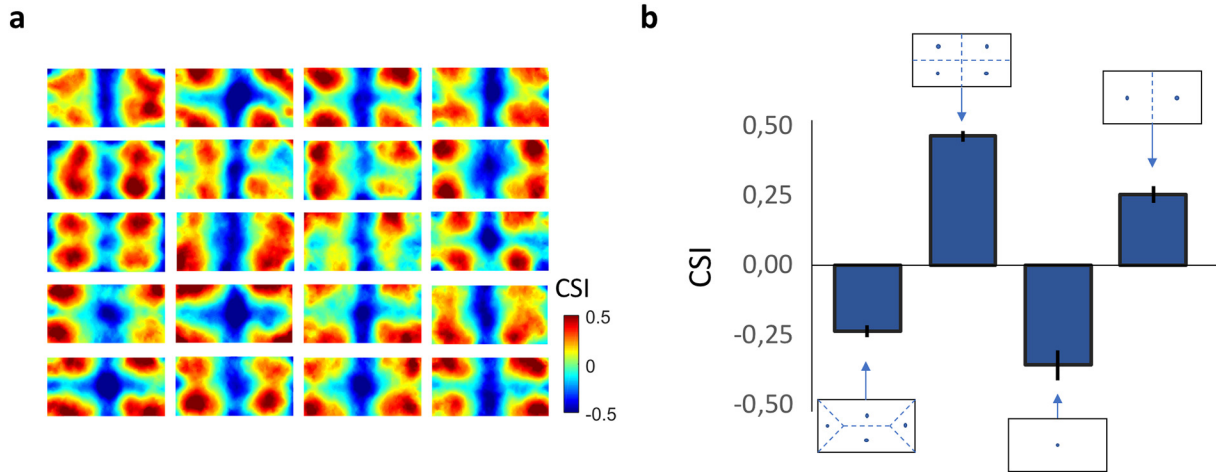
2.2. Results

We used all participant's responses, regardless of the magnitude of the error, and excluded only those responses that were made outside the shape (0.25%). The same analyses, but excluding those responses that were 3 SD above each participants' response mean (1.48%) and responses that were larger than half the maximum size of the shape (0.39%), produced virtually identical results. Fig. 2a (top row) shows the mean error vectors for each stimulus location across participants. The pattern of errors appears to converge to four regions of the rectangle symmetrically situated around each quadrant, as if the rectangle had been divided using an imaginary vertical and a horizontal line crossing at the center. Interestingly, the arrows move away from the center of the figure. This pattern of biases is better characterised in the averaged similarity maps (Fig. 2b, top row; warm colours indicate regions which attract nearby stimuli; cool colours indicate regions which repel nearby stimuli). Four distinct positive red clusters are apparent within the shape, broadly in the center of each of the quadrants resulting from vertical and horizontal bisection of the rectangle, consistent with previous research using circles (Huttenlocher et al., 2004, 1991). Interestingly, there was also a negative central cluster spanning from the upper to the lower side of the figure and dividing the shape into two halves, suggesting it serves as an anti-prototype, repelling stimuli. This might reflect a combined radial bias in the outward direction for targets near the center of the figure and a bias away from the category borders (see Huttenlocher et al., 1991). Remarkably, a similar pattern of biases is identified across single participants (Fig. 3a).
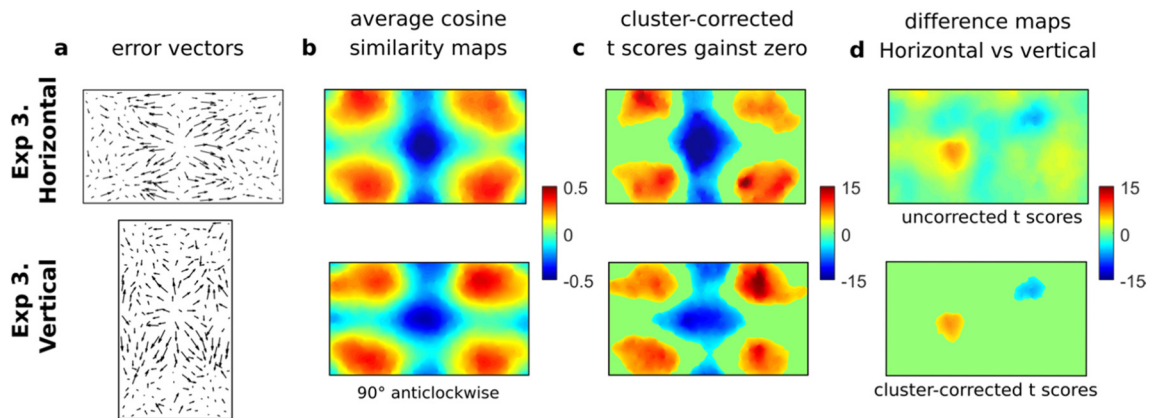
To evaluate which regions of attraction and repulsion were consistent across participants, we ran one-sample *t*-tests against zero for each location in the shape. Fig. 2c (top panel) shows the corresponding t-statistics, displayed as a statistical parametric map, analogous to those used in analysis of neuroimaging data (Friston, Ashburner, Kiebel, Nichols, & Penny, 2007). Our analysis adapted cluster-based methods from neuroimaging to model the spatial relations among statistical tests. We depicted those locations (i.e., pixels) which survived cluster correction for multiple comparisons using a permutation approach (see Analyses section). These analyses revealed five clusters significantly

different from zero, and therefore consistent across participants: the four prototypes typically found in circles (Huttenlocher et al., 2004; Wedell et al., 2007) and a central anti-prototype spanning across the vertical axis of the rectangle.

Finally, we tested the hypothesis that the medial-axis skeletal representation of the shape might play a role in the division of the shape and further categorization. The shape skeleton offers a structurally simplified description of a shape and it has been proposed that it might be used for coding into memory (Kovács & Julesz, 1994; Marr, 1982). Furthermore, Firestone and Scholl (2014), found that when people are asked to point just once to any location inside a shape (including rectangular shapes), their responses are more likely situated at locations consistent with the shape skeleton, which, in a rectangle, it is formed by one inward triangle on each side, and a horizontal line in the middle connecting the two vertices of the triangles (Fig. 3b, first graph bar; Firestone & Scholl, 2014). Based on these results, we could expect responses in the rectangle to be biased towards the center of mass of each polygon obtained after an implicit division using the skeleton (see Analyses section). Our results show that this was not the case. We calculated the mean cosine similarity index for each subject, assuming only these four prototypes, rather than each pixel, as in the data-driven analyses reported so far. We found a negative similarity index of -0.24 across participants (SD = 0.10, one sample *t*-test, t(19) = -10.67, $p \leq 0.001$). This negative similarity index indicates that the four centroids of the skeleton model repel, rather than attract, nearby responses. Note that when performing the same analyses, but assuming the four prototypes to be at the centroids of each quadrant, we obtained a large positive similarity index across subjects of 0.46 (SD = 0.09, one sample t-test, t(19) = 22.66, p ≤ 0.001). This pattern of results further corroborates the idea that people categorize space in four regular quadrants and validates this model-based analysis. For completeness, we tested a model in which there is only one attractor in the geometrical center of the rectangle, assuming a single category (e.g., Sampaio & Cardwell, 2012), and a model in which two prototypes are considered, one at each halve of the rectangle, as if participants would have imposed a vertical boundary in the middle of the shape (e.g., Huttenlocher et al., 1994). As expected, from our previous analyses, a single central prototype produced a negative similarity index across subjects of -0.36 (SD = 0.24, one sample t-test, t(19) = -6.77, $p \leq 0.001$), which reflects part of the central anti-prototype depicted in Fig. 2b. Two prototypes produced a positive similarity index of 0.25 (SD = 0.14, one sample t-test, t (19) = 8.12, $p = 0.001$), but this was statistically smaller than the index obtained using the four centroids as prototypes (paired t-test, t (19) = 7.53, $p \leq 0.001$). Note that the results from model-based analyses are coarser than those obtained with our data-driven method proposed above, as they rely on the usage of specific (i.e., predefined) locations, which might or might not correspond to actual prototypes (e.g., Holden, Newcombe, & Shipley, 2013). Also, the same pattern of

Fig. 3. Cosine similarity maps across subjects in Experiment 1 and results from the model-based analyses. a) Each CSI map represent the data on one participant. Positive values indicate systematic response biases towards these locations. Negative values indicate systematic biases away from these locations. b) Each bar represents the mean CSI when assuming that specific locations serve as prototypes (blue dots). Each rectangle corresponds to a possible configuration of the prototypes, i.e., using the shape skeleton, the four quadrants, a central prototype and two halves. (For interpretation of the references to colour in this figure legend, the reader is referred to the web version of this article.)

Fig. 4. Results of Experiment 3. (a) Mean error vectors across participants. (b) Mean cosine similarity indexes across participants. (c) One-sample *t*-test scores against zero for each location across participants with cluster correction for multiple comparisons. (d) Paired *t*-test scores between horizontal vs vertical orientations, depicting uncorrected (top panel) and cluster corrected t scores for multiple comparisons (bottom panel). The vertical rectangle was rotated 90° anticlockwise to facilitate comparisons.

results and statistics are obained if no weight is given by the error length (CSI skeleton: −0.15, centroids: 0.33, geometrical center: −0.26, two halves: 0.14).

3. Experiment 2: effects are not due to the use of a fixation cross

In Experiment 1, a fixation cross was presented on each trial to signal the location of the center of the first rectangle. This cross center might provide an explicit visualization (through an afterimage or from memory) of the vertical and horizontal axes crossing the shape through the middle, which might have induced or strengthen the division of the shape into four quadrants. To test whether the use of the extrinsic vertical and horizontal was mostly driven by the presence of a cross preceding the first rectangle, we tested the same set of 395 dot locations in a new sample of participants but without any fixation cross.

3.1. Methods

Twenty new volunteers participated in Experiment 2 (M = 27.35 years old, SD = 6.04, 11 females). The materials and procedures were identical to experiment 1, with the exception that the fixation cross was now exchanged by a blank screen.

3.2. Results

We found virtually identical results (see Fig. 2, bottom panels). Two-sample *t*-tests comparing CSI at each location in the rectangle between the two experiments showed that no cluster differed significantly (Fig. 2d). This suggests that the division of the rectangle into vertical and horizontal axes in Experiment 1 was not due to priming from the presence of a fixation cross formed of vertical and horizontal lines.

4. Experiment 3: intrinsic cues define categorical anti-prototypes

In Experiments 1 and 2, we observed a central anti-prototype spanning the vertical axis, which could either reflect an alignment with the extrinsic vertical, or an alignment with the rectangle's shorter axis of symmetry. If the former is true, rotating the shape should change the location of the anti-prototype, which would now be parallel to the long axis of the rectangle. If the latter is true, rotation should have no effect. In Experiment 3, we tested both horizontally- and vertically-oriented rectangles (Fig. 4).

4.1. Methods

Sixteen new volunteers participated in Experiment 3 (M = 27.69 years old, SD = 6.54, 8 females). The materials and procedures were similar to experiment 1, with the following exceptions. First, two types of rectangles, i.e., vertical and horizontal, were presented in different conditions (ABBA design, 21.1° × 10.7°, 825 × 416 pixels). Second, 240 dot locations, rather than 395, were presented. The distribution of dots was selected pseudo-randomly with a minimum distance between dots set to 30 pixels. Dot locations were identical in both orientations, with the horizontal rectangle rotated 90° clockwise. Third, for the cluster-based permutation analysis, neighbouring pixels were considered as a cluster if their individual t values were higher than the critical value ($p < 0.001$; $T_{crit}(15) = 3.73$), which differs from Experiment 1 because the number of participants is different. Finally, the experiment was about 15 min longer.

4.2. Results

We found four significant positive clusters in both orientations, similar in shape and location. The central negative cluster run across the vertical axis in the horizontal rectangle, but along the horizontal axis in the vertical version of it (Fig. 4b). That is, along the short axis in both rectangles, indicating that the central anti-prototype is primarily based on an intrinsic (object-centered) reference frame. Thus, the extrinsic vertical is not the only reference frame in which spatial categories are defined, as might be assumed from the classical results in the circle (Huttenlocher *et al.,* 1991). In the radially-symmetric circle, which lacks unique intrinsic symmetry axes, participants rely on extrinsic cues. When, however, intrinsic properties of the object are available, these cues play a key role in spatial categorization.

Nonetheless, the two rectangles did differ in two small clusters (Fig. 4d), one negative and one positive. The negative cluster simply denoted larger t-values in one of the clusters of the vertical rectangle. More interestingly, the positive cluster indicated the existence of a small anti-prototype parallel to the long axis of the vertical rectangle (aligned with the extrinsic vertical only in this rotation), which was absent in the horizontal rectangle. This emerging positive cluster suggests that the saliency of the vertical axis, which is aligned with gravity (and the retina, and torso), might also, although to a smaller extent, play a role in the way spatial anti-prototypes are defined.

5. Experiments 4: dissociating the influence of extrinsic and intrinsic reference frames

The results of Experiment 3 show that categorical anti-prototypes are influenced by intrinsic cues, such as symmetry axes within a shape. They also suggest interactions between reference frames, by showing that the anti-prototype at one symmetry axis is enhanced when aligned with the extrinsic vertical. The effect exerted by each reference frame in Experiment 3, however, is difficult to interpret, and limited to changes in the strength of biases, as symmetry axes in the two rectangular orientations are aligned to the extrinsic vertical and horizontal. In Experiment 4, we explored the degree to which each reference frame (i.e., extrinsic and intrinsic) plays a role in the actual structure of prototypical biases. To do so, we presented a square and the same square rotated 45° (i.e., a diamond). Unlike the rectangle, the square has four axes of symmetry that differ in their alignment with the extrinsic vertical and horizontal axes across the two orientations. In the non-rotated square, the alignment corresponds to those axes that connect the middle of opposite sides, and in the rotated version, to those that connect opposite corners. Thus, if participants use a purely extrinsic reference frame, and indistinctly impose vertical and horizontal boundaries across orientations, we should observe four prototypes: one at each quadrant in the non-rotated version, and one at each triangle in the rotated version (given that the extrinsic subdivision corresponds to

a division through the corners in this orientation). If, in contrast, participants use a purely intrinsic reference frame, we should observe identical categorical structure across orientations. More specifically, under this hypothesis, we should find a structure of biases explained by a division through the sides in the two orientations (as this is what we expect in the non-rotated square, based on Experiments 1–3). We also included a circle to provide clear evidence in the same participants that extrinsic reference frames are used when intrinsic cues are not available (Huttenlocher *et al.,* 1991).
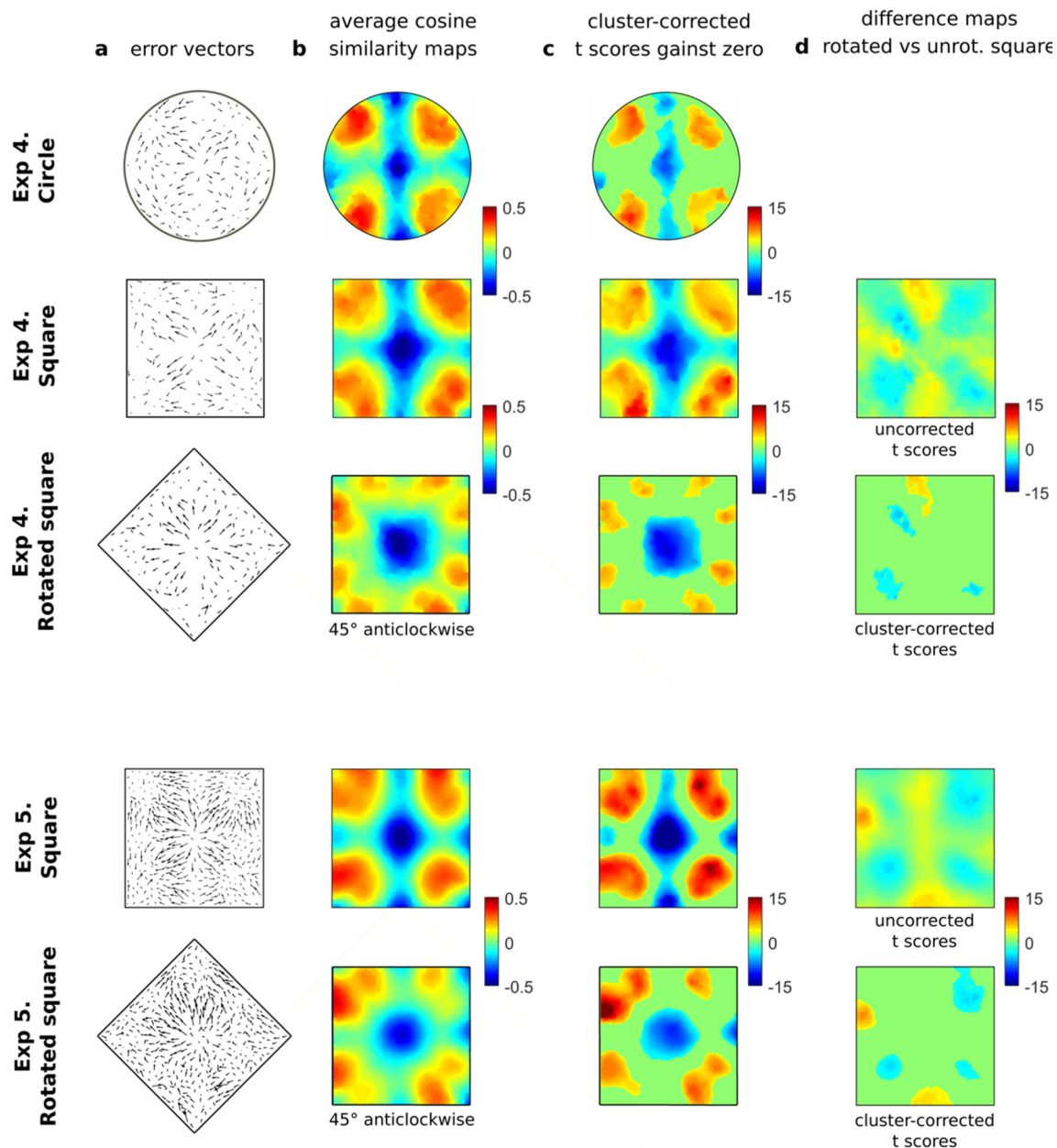
5.1. Methods

Twenty new volunteers participated in Experiment 4 (M = 28.67 years old, SD = 7.24, 9 females). The materials and procedures were similar to experiment 1, with several exceptions. Three conditions were presented in an ABCCBA design, a circle (18.0° in diameter, 700 pixels), a square (15.9° in length, 620 pixels) and the same square rotated 45 deg. Each figure contained 160 different possible dot locations (dots were separated by at least 30 pixels). The Experiment lasted about 1 h 15 min.

In this experiment we conducted further analyses on the CSI maps. In particular, we correlated each participant's CSI maps in the square and rotated-square with two theoretical models each (an aligned model with the extrinsic reference frame and a misaligned model), using Fisher's z-transformation (Fig. 6). For the non-rotated square, the aligned model divided the space within the square using the vertical and horizontal axes of symmetry, which corresponds to those axes that connect the middle of opposite sides (for examples of the models see Fig. 6a, top row). The misaligned model, on the contrary, divided the space within the square using the two oblique axes of symmetry, which corresponds to those axes that connect opposite corners. To create the aligned model, we first created a 100 × 100 pixels matrix of zeros and divided it in four quadrants (the crossing lines were three pixels large). We then individuated the four centroids of each quadrant, and marked them with values of 1 including also neighbouring pixels within an eight-pixels radius. The central point of the image plus a radius of eight pixels was marked with values of −1 to simulate the central anti-prototype. Also, the crossing lines were marked as −1 to simulate the anti-prototypes observed at the categorical borders. Finally, we used a 2D Gaussian filter with a sigma of 16 pixels to smooth the matrix. The model map was then reshaped to the size of the similarity maps. For the misaligned model, we used the same procedure but the matrix was divided by rotating the crossing lines 45 degrees clockwise (i.e., dividing the shape through the corners). The two models were then compared to each participant's similarity maps using correlation coefficient analyses. Each individual Pearson's correlation coefficient was then transformed using Fisher z-transformation to produce a normal distribution of correlations and compare them across models. The averaged correlation coefficients between models and actual maps were submitted to a repeated measure analysis of variance (ANOVA). For the rotated square, we rotated the two models 45° and reversed the names of the models: with the aligned model corresponding now to a division through the corners and the misaligned model to a division through the sides.

5.2. Results

The results are shown in the three top rows of Fig. 5. For the circle and the non-rotated square, the pattern of biases was similar to the rectangle in Experiments 1 to 3. Four positive clusters survived correction for multiple comparisons, suggesting participants imposed vertical and horizontal boundaries dividing the shapes into quadrants (Fig. 5c). For the rotated square, however, at least eight distinct attractors were distinguishable, as if participants divided the shape using all four symmetry boundaries (resulting in eight right-angled triangles, Fig. 5b). All the clusters survived multiple comparison correction

Fig. 5. Results of Experiments 4 (top) and 5 (bottom). (a) Mean error vectors across participants in Experiments 4 (top) and 5 (bottom). (b) Averaged cosine similarity indexes across participants. (c) One-sample *t*-test scores against zero for each location across participants with cluster correction for multiple comparisons. (d) Paired (Experiment 4) and two-sample (Experiment 5) *t*-test scores between the two square orientations, depicting uncorrected (top panel) and cluster corrected t scores for multiple comparisons (bottom panel). Rotated squares are rotated back 45° anticlockwise, to allow for comparison across orientations.
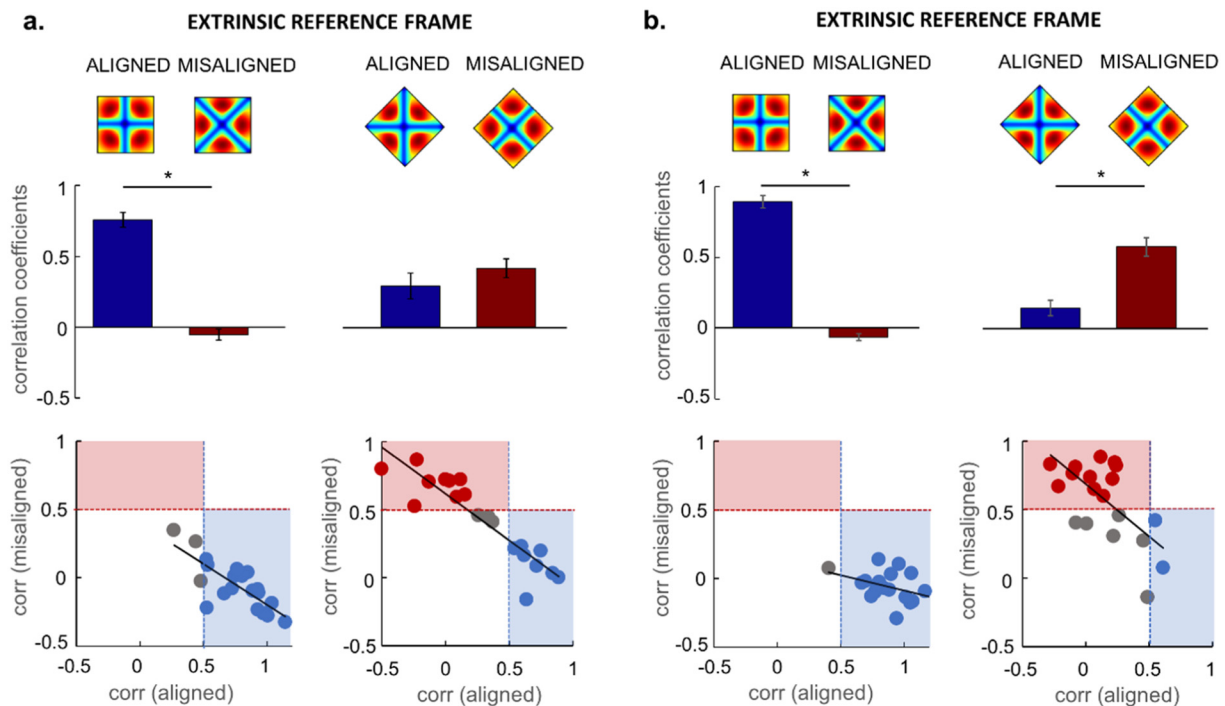
(Fig. 5c). The anti-prototype in the rotated version appeared as a round shape in the middle and lacked any particular direction, in stark contrast to the non-rotated version, where a clear negative cluster ran across the vertical axis (Fig. 5b-c). We compared the two orientations using paired *t*-tests at each location, finding four negative clusters in the proximity of the four angles of the standard square (at an uncorrected $p < 0.001$), three surviving multiple comparison correction, indicating that each of the four prototypes in the standard square was divided into two in the rotated-square (Fig. 5d). A positive cluster located in the upper part of the shape also survived correction, depicting part of the vertical anti-prototype observed only in the non-rotated square. The different number of prototypes observed in the two orientations suggests that participants did not use either a purely extrinsic or a purely intrinsic reference frame, but a combination of the two.

To clarify the role of each reference frame, we correlated each

participant's similarity maps with two theoretical models using Fisher's *z*-transformation (Fig. 6a; correlation across the two models: $r = -0.29$). Both models depict theoretical distributions of biases corresponding either to the use of axes of symmetry *aligned* with the extrinsic vertical and horizontal or to axes of symmetry *misaligned* with those axes. In the non-rotated square, the aligned model corresponds to a division through the sides and the misaligned model to a division through the corners (Fig. 6a, top-left panel). This correspondence is reversed in the rotated version (Fig. 6a, top-right panel).

A repeated measures analysis of variance (ANOVA), using averaged correlation coefficients between models and actual maps, with the factors Orientation (rotated, non-rotated) and Extrinsic Alignment (aligned, misaligned) revealed a main effect of Alignment (F $(1,19) = 15.22$, $p < 0.001$, $\eta_p^2 = 0.44$) and a significant interaction (F $(1,19) = 28.06$, $p < 0.001$, $\eta_p^2 = 0.60$). As shown in Fig. 6a (top-left

Fig. 6. Results of Experiments 4 (a) and 5 (b). The top panels depict the mean correlation coefficient (using Fisher's z transformation) between actual similarity maps and two theoretical distribution of errors. One distribution is always aligned with the extrinsic vertical and horizontal (blue bars) and the other is always misaligned (red bars). The bottom panels depict the linear distribution of correlations across subjects and across the two models (aligned and misaligned). Red panels and dots correspond to Fisher-transformed correlations > 0.5 between actual maps and the misaligned model, and blue, between actual maps and the aligned model. (For interpretation of the references to colour in this figure legend, the reader is referred to the web version of this article.)

panel), in the non-rotated square, the aligned model (blue bars; $r = 0.76$) explained biases better than the misaligned model (red bars; $r = -0.05$; comparison between the two models: t(19) = 9.31, p < 0.001, $d = 2.08$). Indeed, the comparison with the aligned model in all except for three participants produced Fisher's transformed correlations larger than 0.5 (Fig. 6a, bottom-left panel). In contrast, the distribution of biases in the rotated square was indistinctly explained by the aligned ($r = 0.29$) and misaligned models ($r = 0.42$, comparison: t (19) = -0.81, p = .43, $d = -0.18$, Fig. 6a, top-right panel). This null effect is easily spotted in the linear distribution of correlations observed across participants (Fig. 6a, bottom-right panel). It also explains the eight prototypes that emerged in the averaged similarity map, as a result of averaging biases across participants (Fig. 5b, third row). The results of Experiment 4 suggest that when intrinsic cues are available, the vertical and horizontal division does not play such a fundamental role in spatial categorization. While the pattern of biases in the square was consistent with the use of an extrinsic reference frame, this was not the case for the same shape rotated 45°, where participants showed different spatial subdivisions, ranging from weak to strong reliance on symmetry axes aligned with an extrinsic reference frame. In this way, the division of space by imposing vertical and horizontal axes is more nuanced than previously suggested (Engebretson & Huttenlocher, 1996; Huttenlocher et al., 2004; Wedell et al., 2007).

6. Experiment 5: a flexible use of reference frames defines categorical biases

Experiment 4 was embedded in a context where a division of space aligned with the extrinsic axes was ubiquitous. This is so, as participants were exposed to three figures, two of which, the circle and the non-rotated square, were unambiguously divided using vertical and horizontal boundaries. Thus, it is possible that the unclear pattern of biases is the result of interference from preceding encodings/retrievals of locations and therefore subdivisions of space (Crawford & Duffy,

2010). Moreover, in Experiment 4, multiple allocentric cues were freely available e.g., the monitor and the testing room. These cues cannot help retrieving the location of the dot, as shapes moved around the screen, but could nonetheless reinforce the imposition of vertical and horizontal boundaries to categorize the shapes, for instance, by comparing the shape to the edge of the monitor.

In Experiment 5 we removed this interference by presenting only one shape, either a square or a rotated-square, in separate groups of participants rather than separate blocks. Furthermore, we removed the fixation cross, changed the cross-shaped mouse pointer to a hand-shape cursor to avoid any potential priming of vertical and horizontal axes, and removed environment-based frames by asking participants to look at the screen through a black cylinder, blocking any other view than a circular-shaped screen at the end. A different pattern of results across the two experiments would suggest that the weight given to each reference frame is context-dependent and can be flexibly deployed.

6.1. Methods

Forty new volunteers participated in Experiment 5 (non-rotated square: $n = 20$, 24.80 years old, SD = 5.22, 14 females, rotated-square: n = 20, 27.20 years old, SD = 8.68, 12 females). The materials and procedures were similar to experiment 4, with several exceptions. Two groups of participants were tested, rather than one, and were presented with a single shape each, rather than three. One group was presented with a square and a second group with a rotated square (10.7° length, 413 pixels). 425 dot locations were presented one by one in random order. The distribution of dot locations was identical across orientations, with the rotated square rotated 45° clockwise (dots were separated by at least 16 pixels, and each dot measured 7 pixels). In Experiment 5, participants were seated at one end of a cone, with the monitor situated at the other end such that the screen edges were circular rather than rectangular, and the view of the experimental room was blocked. We removed the fixation cross and changed the cross-

shaped mouse pointer to a hand-shape cursor. The experiment lasted about 1 and 1.5 h.

6.2. Results

The results are shown in the bottom two rows of Fig. 5. The pattern of biases was very similar to those obtained in Experiment 4, with the exception that the eight positive clusters in the rotated square were not as clearly defined, as each pair of clusters was interconnected through a few pixels. Seven of these semi-attached clusters survived multiple comparison correction (Fig. 5c, last panel). The comparison across the two orientations of the square revealed three negative clusters in the proximity of the four angles of the shape (Fig. 5d, bottom panel), indicating that at least three of the four prototypes found in the non-rotated square were partially divided into two, when rotated. Two positive clusters located in the central lower and left parts also survived the correction. One of them denoting a trivial change in the strength of bias found across orientations in one of the prototypes, and the other, reflecting part of the vertical anti-prototype observed only in the non-rotated square.

A mixed ANOVA using the averaged correlation coefficients (Fisher's z transformation) between models (aligned and misaligned) and actual maps, with Orientation and Alignment as between- and within-subject factors, respectively, revealed a main effect of Alignment ($F(1,38) = 17.72$, $p < 0.001$, $\eta_p^2 = 0.32$) and a significant interaction ($F(1,38) = 123.92$, $p < .001$, $\eta_p^2 = 0.76$). As in Experiment 4, in the non-rotated square, the aligned model ($r = 0.89$) explained categorical biases better than the misaligned model ($r = -0.06$; comparison between the two models: $t(19) = 16.38$, $p < 0.001$, $d = 3.66$, Fig. 6b, top-left panel). Indeed, the comparison between actual maps and aligned model in all except for one participant ($r = 0.41$), produced biases highly correlated ($r > 0.66$, Fig. 6b, bottom-left panel). Importantly, and contrary to Experiment 4, the misaligned model ($r = 0.57$) explained the distribution of biases in the rotated square better than the aligned model ($r = 0.14$, comparison: $t(19) = -3.92$, $p < 0.001$, $d = -0.88$, Fig. 6b, top-right panel). Note that the aligned model in the standard square (i.e., imposing vertical and horizontal boundaries), and the misaligned model in the rotated version (i.e., imposing diagonal boundaries), corresponds to a division through the same axes, i.e., the "side" axes of symmetry. This shift in the distribution of responses as compared to Experiment 4 is clearly visible in the bottom panels of Fig. 6a and b, where individual correlations in the non-rotated square shifted to a greater extent towards the aligned model in Experiment 5 as compared to 4, and towards the misaligned model in the rotated version. This change in the pattern of biases across experiments is also observed in the average similarity matrix of the rotated square, where the eight prototypes, clearly differentiated in Experiment 4, tended to fuse in the present experiment.

The results of Experiment 5 support the idea that participants do not rely on a purely extrinsic reference frame, but the weight given to each reference frame can be modulated depending on the shape and context, and possibly by stable individual differences. Finally, the results of Experiment 5 show a preference for an intrinsic reference frame when extrinsic cues are restricted. In Experiment 5, participants divided the shape across orientations mostly through the same symmetry axes, supporting a major role of the intrinsic reference frame over the extrinsic one. Nonetheless, the fact that the effect of these axes was stronger in the non-rotated than the rotated square (which is reflected in a main effect of Alignment), suggest that the alignment with the extrinsic vertical plays also a central role, an idea that was already sightseen in Experiment 3.

The reason for why one type of intrinsic cue, in this case the symmetry axes dividing the shape through each side, is preferred over those axes dividing the shape through each corner, is an open question. One possible explanation is that there is a genuine preference for these axes of symmetry in the most typical orientation (the non-rotated square),

driven by its alignment with the extrinsic vertical and the salience of vertical lines (Furmanski & Engel, 2000; Wakita, 2012). Constant exposure to, and categorical formation of prototypes in this particular orientation, might prime the imposition of the same intrinsic axes in other orientations.

7. Discussion

Our method provides a form of 'imaging' of the internal category structure of mental representations of shape, and at the same time offers an approach to test them statistically. We used this procedure to map spatial categories in detail for a variety of simple geometric shapes, and to probe the different frames of reference in which these spatial categories operate. Consistent with previous work, memories of dot locations in a rectangle, a square, and a circle were attracted to the centroids of each quadrant. At first glance, the pattern of biases in the three shapes is consistent with the view that a universal division of space, imposing vertical and horizontal boundaries, forms the basis for spatial categorization (Engebretson & Huttenlocher, 1996; Huttenlocher et al., 2004; Wedell et al., 2007). However, our results with rotated shapes, where extrinsic and intrinsic cues are dissociated, challenge this idea by showing that, under certain contexts (e.g., with a diamond shape), some participants rely mostly on cues intrinsic to the shape itself, undermining the idea that vertical and horizontal meridians are used by default.

Our latter findings suggest a flexible, context-dependent, deployment of reference frames. When participants were exposed to the two square orientations, plus a circle, in consecutive blocks, the overall pattern of categorical biases for the rotated-square showed no preference for one reference frame over the other. However, when allocentric environmental cues (e.g., the edge of the monitor, or the pointer cross) and the history of recent categorizations related to the presence of other shapes were removed in Experiment 5, the pattern of categorical biases was very similar across orientations, favouring the use of an intrinsic reference system for most participants. That is, overall, participants divided the shape through the middle of each side. This flexibility contrasts with previous research on spatial categorization, showing that default categories in the circle are very robust and difficult to overcome (Huttenlocher et al., 2004; Lipinski, Simmering, Johnson, & Spencer, 2010; Sampaio & Wang, 2010, see also Spencer & Hund, 2002). In particular, Huttenlocher et al., (2004) showed that category biases persisted regardless of the target distribution, even when the full distribution of locations was made explicit to the participant. In one experiment, for instance, participants were presented with the full distribution of dots, occupying only the surroundings of the vertical and horizontal axes, right before the presentation of the target dot. They found that participants kept imposing vertical and horizontal boundaries (i.e., showing one prototype at each quadrant), even though no dot was ever presented on the proximities of each quadrant. In contrast, we found a fast re-shaping of categorical biases across subjects, where the simple presentation of other shapes in Experiment 4 (or the introduction of basic extrinsic environmental cues), enhanced one reference frame over other as compared to Experiment 5 where only one shape was presented (see Fitting et al., 2005, for the effect of field rotation when peripheral cues are available). Thus, it is possible that this form of categorization is more flexible than previously thought, as long as the object can be subdivided using intrinsic cues and not only extrinsic cues, as in the case of the circle.

Our results instead are consistent with the idea that spatial memories are organized using intrinsic reference systems (McNamara, 2003; Mou et al., 2008a; Mou, et al., 2008b; Wang et al., 2005; Xiao, Mou, & McNamara, 2009). According to this view, people use intrinsic frames of reference of an object to encode and retrieve other objects whenever intrinsic cues are present or evident. In particular, individuals would primarily use an intrinsic reference frame to encode the location of objects organized as a regular layout, and would resort to extrinsic

frames of reference whenever intrinsic cues are not evident because the layout is not regular (Xiao et al., 2009). Individual objects can also have intrinsic directional axes of reference (Tamborello et al., 2012; Wang et al., 2005) that are used to mentally represent the configuration of potential targets around the reference object. Interestingly, these intrinsic frames of reference are especially used when the task is sufficiently easy (Wang et al., 2005). Furthermore, an object or scene often invite the use of multiple intrinsic reference frames, either because there are conflicting situations or ambiguous infromation (Tamborello et al., 2012) or because certain cues are more salient than others (Wang, Johnson, & Zhang, 2001). This line of research indicates that the type of reference frame used to encode and retrieve information in memory is not fixed but depends on various factors such as the task or the saliency of the environmental cues.

We also showed clear anti-prototypes running along the vertical axis and with less strength, along the horizontal one, in the rectangle, the circle, and the non-rotated square. We were therefore able to image these hidden subdivisions for the first time, which likely reflect the borders of each category (e.g., each quadrant). It has been argued that vertical and horizontal axes are imposed by default and are difficult to overcome because they provide category boundaries that are more precise than other boundaries (such as diagonals; Engebretson & Huttenlocher, 1996; Huttenlocher et al., 2004). This comes from the idea that symmetry detection is better around the vertical than the diagonal axis (Engebretson & Huttenlocher, 1996), and humans and monkeys exhibit greater sensitivity to vertical and horizontal than to oblique lines (Wakita, 2012; Wenderoth, 1994). Better symmetry detection at the verticals, therefore, would translate into reduced misclassification of stimuli into other categories (in this case quadrants) producing a larger bias away from the vertical (Engebretson & Huttenlocher, 1996; Schmidt, 2004). Boundary precision could explain why we observed larger anti-prototypes at the vertical as compared to the horizontal axis. However, the idea that boundary precision, per se, is a major factor in the imposition of vertical and horizontal boundaries is challenged by our results in the rotated square. This challenge comes from the fact that corners in the rotated square are unbiased landmarks of the actual location of the vertical and horizontal axes (at least in a gravitational frame of reference), which should produce little, if any, misclassification of stimuli into other categories, yet participants nonetheless imposed boundaries at the sides and not the corners of the rotated square.

The finding that intrinsic properties of a shape directly affect categorical biases brings into question whether the prototype structure we find relates to existing algorithms for identifying internal or 'skeletal' structure within objects. Blum (1973), for example, introduced the idea of the medial-axis skeleton, and developed the so-called grassfire algorithm for calculating it. In a rectangle, the medial axis skeleton is formed by one inward triangle on each side, and a horizontal line in the middle connecting the two vertices of the triangles (Firestone & Scholl, 2014, see Fig. 3b). This shape skeleton might offer a structurally simplified description of the shape which can be used for coding into memory (Kovács & Julesz, 1994). Other approaches to identifying skeletal structure within shapes have also been developed, such as Feldman and Singh's (2006) Bayesian approach, which attempts to balance fit to the exact details of the shape with skeleton complexity. In the case of a rectangle, this latter model gives a skeleton consisting of a single line in the center of the rectangle aligned with the rectangle's long axis. It is noteworthy, however, that neither of these skeletal representations has any apparent connection to the pattern of spatial prototypes that we identify.

Langlois et al. (2017) recently found that angular shapes show bimodal peaks (i.e., prototypes) at the vertices. In principle, one could argue that the eight-prototype pattern found in Experiment 4 and to a lesser extent in Experiment 5, reflect intrinsic bimodal peaks linked to the presence of a vertex. However, the absence of bimodal peaks in the rectangle and square suggests that the effect is driven by the actual rotation of the shape and hence a combined use of reference frames across participants. Note that in Langlois et al.'s study, the pattern of errors is the result of bias accumulated and passed along a chain of participants (i.e., using the method of serial reproduction), thus it is unknown whether bimodal peaks would still be observed in a within-subject design.

Finally, several studies have investigated categorical biases in the recall of locations within natural scenes (such as scenes of geological interest or in real outdoor settings; Holden, Curby, Newcombe, & Shipley, 2010; Holden, Newcombe, Resnick, & Shipley, 2015; Holden et al., 2013). Overall, these studies suggest that memory for locations is biased towards the prototype. However, in these studies, a central prototype (center of mass) of a proposed category is always assumed. Thus, the actual structure of categories and prototypes remains hidden in these studies. Our approach could prove relevant to fill this gap and depict a complete structure of shape categories. For instance, using this method, we have recently been able to extract complex patterns of categorical biases in non-geometrical shapes, such as in pictures of faces and bodies (data unpublished), which would have been overlooked with previous methods.

To conclude, we provided a detailed description of a new method for 'imaging' and testing the internal structure underlying spatial representation of objects. This allowed us to visualise spatial biases and map the mental spatial prototypes and divisions used to localize events from memory with a level of detail never previously reported. Furthermore, we showed that the internal structure of the investigated shapes is not only defined by information extrinsic to shape (e.g., retina- or gravity-based), but also by cues intrinsic to shape (e.g. the axes of symmetry). These results are important as they provide new information to explain how people divide the internal space of geometrical shapes. Furthermore, our results suggest that our approach can be used to 'image' the internal structure of shape categories for a wide range of perceptual phenomena, even across irregular shapes. This could allow measurement of categorical biases in spatial memory using natural scenes, or biologically-related stimuli, such as faces or bodies.

Supplementary data

The full dataset for this study is available to download at https://osf.io/zvq6f/.

CRediT authorship contribution statement

Elena Azañón: Conceptualization, Methodology, Formal analysis, Writing - original draft, Writing - review & editing.**Raffaele Tucciarelli:**Conceptualization, Methodology, Formal analysis, Writing - original draft, Writing - review & editing.**Metodi Siromahov:**Investigation.**Elena Amoruso:**Investigation.**Matthew R. Longo:**Conceptualization, Methodology, Formal analysis, Writing - original draft, Writing - review & editing, Supervision.

Acknowledgements

References

Appelle, S. (1972). Perception and discrimination as a function of stimulus orientation: The "oblique effect" in man and animals. *Psychological Bulletin, 78*(4), 266–278. https://doi.org/10.1037/h0033117.

Blum, H. (1973). Biological shape and visual science (part I). *Journal of Theoretical Biology, 38*, 205–287.

Cheng, K., Shettleworth, S. J., Huttenlocher, J., & Rieser, J. J. (2007). Bayesian integration of spatial information. *Psychological Bulletin, 133*(4), 625–637. https://doi.org/10.1037/0033-2909.133.4.625.

Crawford, L. E., & Duffy, S. (2010). Sequence effects in estimating spatial location. *Psychonomic Bulletin & Review, 17*(5), 725–730. https://doi.org/10.3758/PBR.17.5.

725.

Duffy, S., Huttenlocher, J., & Elizabeth Crawford, L. (2006). Children use categories to maximize accuracy in estimation. *Developmental Science, 9*(6), 597–603. https://doi.org/10.1111/j.1467-7687.2006.00538.x.

Engebretson, P. H., & Huttenlocher, J. (1996). Bias in spatial location due to categorization: Comment on Tversky and Schiano. *Journal of Experimental Psychology. General, 125*(1), 96–108.

Feldman, J., & Singh, M. (2006). Bayesian estimation of the shape skeleton. *Proceedings of the National Academy of Sciences of the United States of America, 103*(47), 18014–18019. https://doi.org/10.1073/pnas.0608811103.

Firestone, C., & Scholl, B. J. (2014). "Please tap the shape, anywhere you like": Shape skeletons in human vision revealed by an exceedingly simple measure. *Psychological Science, 25*(2), 377–386. https://doi.org/10.1177/0956797613507584.

Fitting, S., Wedell, D. H., & Allen, G. L. (2005). Memory for spatial location: Influences of environmental cues and task field rotation. In A. G. Cohn, & D. M. Mark (Vol. Eds.), *Spatial information theory. COSIT 2005. Lecture notes in computer science. Vol. 3693. Spatial information theory. COSIT 2005. Lecture notes in computer science* (pp. 459–474). Berlin, Heidelberg: Springer. https://doi.org/10.1007/11556114_29.

Fitting, S., Wedell, D. H., & Allen, G. L. (2007). Memory for spatial location: Cue effects as a function of field rotation. *Memory & Cognition, 35*(7), 1641–1658. https://doi.org/10.3758/BF03193498.

Friston, K., Ashburner, J., Kiebel, S., Nichols, T., & Penny, W. (2007). *Statistical parametric mapping. The analyses of functional brain images.* Academic Press.

Furmanski, C. S., & Engel, S. A. (2000). An oblique effect in human primary visual cortex. *Nature Neuroscience, 3*(6), 535–536. https://doi.org/10.1038/75702.

Harnad, S. (Ed.). (1987). *Categorical perception: The groundwork of cognition.* Cambridge University Press.

Holden, M. P., Curby, K. M., Newcombe, N. S., & Shipley, T. F. (2010). A category adjustment approach to memory for spatial location in natural scenes. *Journal of Experimental Psychology. Learning, Memory, and Cognition, 36*(3), 590–604. https://doi.org/10.1037/a0019293.

Holden, M. P., Newcombe, N. S., Resnick, I., & Shipley, T. F. (2015). Seeing like a geologist: Bayesian use of expert categories in location memory. *Cognitive Science, 40*, 440–454. https://doi.org/10.1111/cogs.12229.

Holden, M. P., Newcombe, N. S., & Shipley, T. F. (2013). Location memory in the real world: Category adjustment effects in 3-dimensional space. *Cognition, 128*(1), 45–55. https://doi.org/10.1016/j.cognition.2013.02.016.

Huttenlocher, J., Hedges, L. V., Corrigan, B., & Crawford, L. E. (2004). Spatial categories and the estimation of location. *Cognition, 93*(2), 75–97. https://doi.org/10.1016/j.cognition.2003.10.006.

Huttenlocher, J., Hedges, L. V., & Duncan, S. (1991). Categories and particulars: Prototype effects in estimating spatial location. *Psychological Review, 98*, 352–376.

Huttenlocher, J., Newcombe, N., & Sandberg, E. H. (1994). The coding of spatial location in young children. *Cognitive Psychology, 27*(2), 115–147. https://doi.org/10.1006/cogp.1994.1014.

Kleiner, M., Brainard, D., & Pelli, D. (2007). *What's new in psychtoolbox-3? Perception 36 ECVP abstract supplement.*

Kovács, I., & Julesz, B. (1994). Perceptual sensitivity maps within globally defined visual shapes. *Nature, 370*, 644–646.

Kuhl, P. K. (1991). Human adults and human infants show a "perceptual magnet effect" for the prototypes of speech categories, monkeys do not. *Perception & Psychophysics, 50*(2), 93–107. https://doi.org/10.3758/BF03212211.

Langlois, T. A., Suchow, J., & Griffiths, T. L. (2017). Uncovering visual priors in spatial memory using serial reproduction. *Proceedings of the 39th annual meeting of the cognitive science seociety* (pp. 712–717). .

Lipinski, J., Simmering, V. R., Johnson, J. S., & Spencer, J. P. (2010). The role of experience in location estimation: Target distributions shift location memory biases. *Cognition, 115*(1), 147–153. https://doi.org/10.1016/j.cognition.2009.12.008.

Lowe, D. (1987). Three-dimensional object recognition from single two dimensional images. *Artificial Intelligence, 31*, 355–395.

Maris, E., & Oostenveld, R. (2007). Nonparametric statistical testing of EEG- and MEG-data. *Journal of Neuroscience Methods, 164*(1), 177–190. https://doi.org/10.1016/j.jneumeth.2007.03.024.

Marr, D., & Nishihara, H. K. (1978). Representation and recognition of the spatial organization of three-dimensional shapes. *Proceedings of the Royal Society of London B, 207*, 187–217.

Marr, D. (1982). *Vision: A computational investigation into the human representation and processing of visual information.* New York: W. H. Freeman.

McNamara, T. P. (2003). How are the locations of objects in the environment represented in memory? *Cognition,* 174–191. https://doi.org/10.1007/3-540-45004-1_11.

Mou, W., Fan, Y., McNamara, T. P., & Owen, C. B. (2008a). Intrinsic frames of reference and egocentric viewpoints in scene recognition. *Cognition, 106*(2), 750–769. https://doi.org/10.1016/j.cognition.2007.04.009.

Mou, W., Xiao, C., & McNamara, T. P. (2008b). Reference directions and reference objects in spatial memory of a briefly viewed layout. *Cognition, 108*(1), 136–154. https://doi.org/10.1016/j.cognition.2008.02.004.

Newcombe, N., Huttenlocher, J., & Learmonth, A. (1999). Infants' coding of location in continuous space. *Infant Behavior and Development, 22*(4), 483–510. https://doi.org/10.1016/S0163-6383(00)00011-4.

Newcombe, N. S., & Huttenlocher, J. (2000). *Making space. The development of spatial representations and reasoning.* Cambridge, MA, US: The MIT Press.

Nichols, T. E., & Holmes, A. P. (2002). Nonparametric permutation tests for functional neuroimaging: A primer with examples. *Human Brain Mapping, 15*(1), 1–25. https://doi.org/10.1002/hbm.1058.

Palmer, S. E., & Hemenway, K. (1978). Orientation and symmetry: Effects of multiple, rotational, and near symmetries. *Journal of Experimental Psychology: Human Perception and Performance, 4*(4), 691–702. https://doi.org/10.1037/0096-1523.4.4.691.

Sampaio, C., & Cardwell, B. A. (2012). Biases in long-term location memory in the real world. *Quarterly Journal of Experimental Psychology, 65*(10), 1865–1871. https://doi.org/10.1080/17470218.2012.696120.

Sampaio, C., & Wang, R. F. (2010). Overcoming default categorical bias in spatial memory. *Memory & Cognition, 38*(8), 1041–1048. https://doi.org/10.3758/MC.38.8.1041.

Sargent, J., Dopkins, S., & Philbeck, J. (2011). Dynamic category structure in spatial memory. *Psychonomic Bulletin & Review, 18*(6), 1105–1112. https://doi.org/10.3758/s13423-011-0139-0.

Schmidt, T. (2004). Spatial distortions in visual short-term memory: Interplay of intrinsic and extrinsic reference systems. *Spatial Cognition & Computation, 4*(4), 313–336. https://doi.org/10.1207/s15427633scc0404_2.

Spencer, J. P., & Hund, A. M. (2002). Prototypes and particulars: Geometric and experience-dependent spatial categories. *Journal of Experimental Psychology: General, 131*(1), 16–37. https://doi.org/10.1037/0096-3445.131.1.16.

Spencer, J. P., Simmering, V. R., & Schutte, A. R. (2006). Toward a formal theory of flexible spatial behavior: Geometric category biases generalize across pointing and verbal response types. *Journal of Experimental Psychology. Human Perception and Performance, 32*(2), 473–490. https://doi.org/10.1037/0096-1523.32.2.473.

Tamborello, F. P., Sun, Y., & Wang, H. (2012). Spatial reasoning with multiple intrinsic frames of reference. *Experimental Psychology, 59*(1), 3–10. https://doi.org/10.1027/1618-3169/a000119.

Taylor, M. M. (1961). Effect of anchoring and distance perception on the reproduction of forms. *Perceptual and Motor Skills, 12*(2), 203–230. https://doi.org/10.2466/pms.1961.12.2.203.

Wakita, M. (2012). Monkeys perceive the orientation of objects relative to the vertical axis. *Animal Cognition, 15*(6), 1205–1209. https://doi.org/10.1007/s10071-012-0535-5.

Wang, H., Johnson, T. R., & Zhang, J. (2001). The mind's views of space. *Proceedings of the third international conference on cognitive science* (pp. 191–198). .

Wang, H., Sun, Y., Johnson, T. R., & Yuan, Y. (2005). Prioritized spatial updating in the intrinsic frame of reference. *Spatial Cognition & Computation, 5*(1), 89–113. https://doi.org/10.1207/s15427633scc0501_4.

Wedell, D. H., Fitting, S., & Allen, G. L. (2007). Shape effects on memory for location. *Psychonomic Bulletin & Review, 14*(4), 681–686. https://doi.org/10.3758/BF03196821.

Wenderoth, P. (1994). The salience of vertical symmetry. *Perception, 23*, 221–236.

Xiao, C., Mou, W., & McNamara, T. P. (2009). Use of self-to-object and object-to-object spatial relations in locomotion. *Journal of Experimental Psychology: Learning Memory and Cognition, 35*(5), 1137–1147. https://doi.org/10.1037/a0016273.